Efficient Production of Fast Electrons from Femtosecond Laser Interaction with Solid Targets

Paul Gibbon
Centre d'Etudes de Saclay, DRECAM, Service de Photons Atomes et Molecules, Bâtiment 522, 91191 Gif-sur-Yvette, France
(Received 18 January 1994)

The interaction of intense, p-polarized, femtosecond laser pulses with solid-density plasma targets is studied with particle-in-cell simulation. At large angles of incidence the density profile is rapidly modified by a "push-pull" combination of ponderomotive force and the space-charge effect of electrons held outside the solid, eventually leading to efficient absorption over a wide range of laser irradiance. For $I\lambda^2 > 10^{17}$ W cm^{-2} μm^2, the *final* absorption rate peaks at 45°–50° and is largely independent of intensity; the *average* absorption fraction and the shape of the fast electron distribution both depend on the ratio of the pulse length to the ion shelf expansion time $t_s \propto \omega_0^{-1}(m_i/Zm_e)^{1/2}$.

PACS numbers: 52.40.Nk, 52.50.Jm, 52.65.+z

The study of sub-ps laser interaction with solid targets has entered a challenging phase now that laser irradiances exceeding 10^{16} W cm^{-2} μm^2 can be achieved with table-top systems [1]. These experiments could lead to a compact, efficient source of incoherent x rays, and also provide a promising route to the production of coherent extreme UV or x-ray radiation either from harmonics in the light reflected from the surface [2] or via direct inversion [3]. Incoherent radiation arises from electrons which are accelerated to keV–MeV energies in the vacuum-plasma interface layer created early on in the interaction. Fast electron generation by fs pulses has also been proposed as part of a novel fusion ignition scheme [4].

The problem of laser energy deposition has naturally attracted a great deal of debate over the fs-solid interaction physics, particularly whether significant absorption is at all possible for intense, pedestal-free pulses on high-density steplike profiles. At low irradiances, say $I\lambda^2 \leq 10^{15}$ W cm^{-2} μm^2, the experimental results are broadly consistent with collisional absorption theory [5]. At higher irradiances, however, it is now evident that a number of *collisionless* processes come into play —particularly for obliquely incident, p-polarized light, such as resonance absorption [6], vacuum heating [7–9], and anomalous skin-layer heating [10]. In the limit $v_{\rm osc}/c \gg 1$, heating is also possible at normal incidence via the $\langle v \wedge B \rangle$ force at twice the laser frequency [11–13].

Limited time resolution of present experimental diagnostics on the sub-ps time scale means that information can be obtained mainly about *time-integrated* quantities such as the global absorption rate, average plasma temperature, fast electron/ion populations, and energies. For p-polarized interactions, however, it is the instantaneous density profile which largely dictates the absorption physics. Assuming that the target gets sufficiently ionized early on in the interaction to form a critical surface, the ratio of the radiation and plasma pressures $P_{\rm osc}/P_e = \mu_0 B^2/n_e k T_e$ will determine whether the bulk plasma $n_e > n_c$ expands or steepens during the interaction [14]. On the other hand, electrons pulled out from the surface [7] will tend to drag ions with them—an effect which was essentially excluded from recent simulations at *normal* incidence [11,12]. In this Letter, a quantitative model of fast electron absorption is developed—based on a combination of particle-in-cell simulation and heuristic arguments—which takes the oblique-incidence ion dynamics into account explicitly.

The essential findings of this study are the following: (i) a kinetically driven "push-pull" modification of the density profile leading to the rapid creation of an underdense shelf, and a shock propagating into the target; (ii) a final quasi steady state characterized either by a turbulent form of resonant absorption or by efficient mode vacuum heating [7,8], depending on the ultimate value of $v_{\rm osc}/\omega_0 L$; (iii) a qualitative change in the fast electron population from beamlike to bi-Maxwellian as the shelf develops.

The starting point for these simulations is an overdense plasma step profile, with density n_e/n_c = 2–10, temperatures T_e = 1–2.5 keV, T_e/T_i =3–5, and mass ratio m_i/Zm_e = 1836. Typically 32×10^3–64×10^3 electrons and ions and 1000–4000 grid points were used, depending on the required resolution and system size [(3–6)λ_0]. An electromagnetic wave is launched (in x) from the left-hand boundary and ramped up to a constant amplitude over several laser periods. Oblique incidence is handled by making a relativistic boost to a frame moving with $v_y = c\sin\theta$ perpendicular to the density gradient, as described in a previous work [8]. Let us first consider the initial situation in which the ions are immobile and electrons are pulled out into vacuum by the component of E field normal to the target. Some of these return to the solid and are absorbed as in Brunel's model [7], but others are held outside by a time-averaged $v \wedge B$ force acting *away* from the target; the ensuing charge separation produces a strong dc E field which inhibits further exits from the plasma; see Fig. 1. This is why the absorption fraction decreases with intensity if the density

0031-9007/94/73(5)/664(4)$06.00
© 1994 The American Physical Society

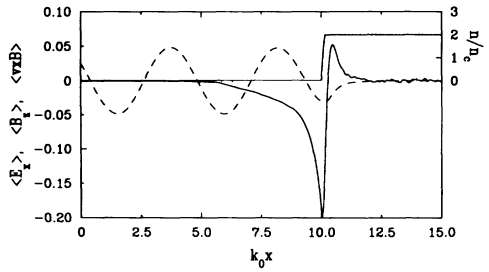

FIG. 1. Initial time-averaged (dc) fields $\langle E_x \rangle$ (solid), $\langle B_z \rangle$ (dotted), and ponderomotive force $\langle v \wedge B \rangle$ (dashed) for $\theta = 45°$, $I\lambda^2 = 10^{17}$, $n/n_c = 2$, and $T_e = 2.5$ keV.

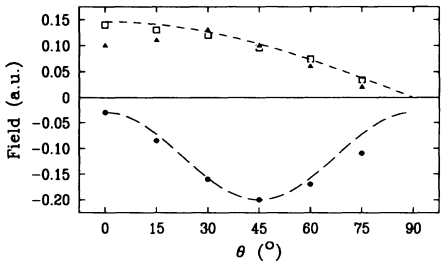

FIG. 2. Initial dc fields into the target (triangles, scaled $\times 2$), away from the target (dots), and ponderomotive force (squares, $\times 2$) as a function of θ. The upper dashed curve ($\times 2$) is the analytical result for the ponderomotive force $v_{\rm osc}^2 \cos\theta$; the lower one is an empirical fit of the form $E_{\rm min} = E_0 + E_1 \sin^2\theta$. The other parameters are as for Fig. 1.

profile is held fixed [8].

This initial configuration should be contrasted with that for normal incidence, where the electrons remain essentially inside the solid, and the ponderomotive force acts only into the target. The angular dependence of the field amplitudes is shown in Fig. 2, which shows that the outwardly directed dc E field peaks at 45°, whereas the inward component actually peaks around 25°. This implies that the shock should be slightly enhanced at finite angles of incidence.

The same dc field that holds electrons inside the target also pulls ions out. An ion falling through the potential $e\Phi = e^2E^2/m_e\omega_0^2$ corresponding to the standing-wave field in Fig. 1 will acquire a velocity $v_i \sim (Zm_e/m_i)^{\frac{1}{2}} v_{\rm osc}$ away from the target. Meanwhile, the inwardly directed ponderomotive force pushes on the overdense plasma: Thermal expansion will be hindered for $v_{\rm osc}^2/v_{te}^2 \gtrsim 2$, whereas for $v_{\rm osc}^2/v_{te}^2 > n_e/n_c$, a shock will develop with front velocity $v_s \sim (n_c/n_e)(Zm_e/m_i \cos\theta)^{\frac{1}{2}} v_{\rm osc}$ [11,12,15].

The push-pull dynamic experienced by the ions distinguishes oblique, p-polarized short-pulse interactions from those with s-polarized or normally incident light, where the profile is steepened, but the shelf forms much more slowly, if at all, and creates the conditions for either resonance absorption or efficient vacuum heating depending on the ultimate value of $v_{\rm osc}/\omega_0 L$. The final steepened profiles found in early 2D simulations [16] on "long-pulse" resonance absorption, starting with $L/\lambda > 1$, also resemble the step-shelf profiles considered here.

Two scenarios are demonstrated by mobile-ion simulations with different laser irradiances, $I\lambda^2 = 4 \times 10^{15}$ and 10^{18} W cm^{-2} μm^2. In both cases the absorption rate increases as the ion shelf develops, saturating after a well-defined period; see Fig. 3. This buildup time, t_s, can be estimated from simple energetic arguments, by assuming that the absorption efficiency is directly correlated to the shelf expansion. For $P_{\rm osc}/P_e \ll 1$, the expansion would be driven by thermal pressure, in which case the density scale length $L \sim c_s t_s$, where $c_s = \sqrt{ZkT_e/m_i}$. Resonance absorption should therefore take place when the scale length $L > 2v_{\rm osc}/\omega_0$, or after a time $\omega_0 t_s \simeq 2v_{\rm osc}/c_s \simeq 2(m_i/Zm_e)^{1/2} v_{\rm osc}/v_{te}$. In practice, for $I\lambda^2 < 10^{16}$, we find a weaker scaling with $v_{\rm osc}$ than this because the ponderomotive force already begins to impede the expansion at the critical surface for $v_{\rm osc}/v_{te} \sim 0.2$, the lowest intensity considered.

In the opposite limit, $P_{\rm osc}/P_e \gg 1$, the electrons pull the ions out via the induced dc field, $E_v = \langle E_x \rangle$, of Fig. 2 given by $e\Phi = e\int E_v\, dx \simeq eE_v X_{\rm osc}$, where $X_{\rm osc} = 2v_{\rm osc}/\omega_0$ is the effective excursion length of the vacuum electrons and Φ is the ponderomotive potential as defined earlier. Thus, $E_v \simeq E_0/2$—a scaling readily confirmed by repeating the simulations of Fig. 2 for different $v_{\rm osc}$. The ion equation of motion can then be integrated, following a fluid element pulled away from the solid, to give an estimate for the expansion time $t_s^2 = 4(m_i/Zm_e)\Delta X_s/\omega_0 v_{\rm osc}$, where ΔX_s is the shelf extension. As the expansion proceeds, the field E_v is carried outwards into the shelf: The barrier which initially prevents efficient vacuum heating will thus be removed when $\Delta X_s \sim 2v_{\rm osc}/\omega_0$. Hence we should have optimum absorption after a time

$$\omega_0 t_s \simeq \sqrt{8}(m_i/Zm_e)^{1/2}, \qquad (1)$$

independent of laser intensity. This result is verified in

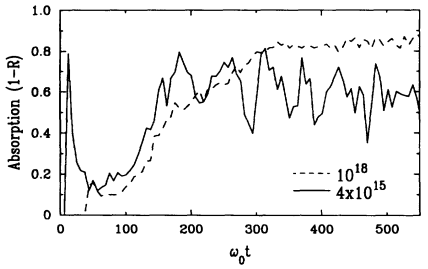

FIG. 3. Time evolution of absorption fraction for $I\lambda^2 = 4 \times 10^{15}$ (solid) and $I\lambda^2 = 10^{18}$ (dashed). The other simulation parameters were $\theta = 45°$, $m_i/Zm_e = 1836$, $T_e = 2.5$ keV, $T_e/T_i = 3$, $n_e/n_c = 5$ (solid), and 10 (dashed).

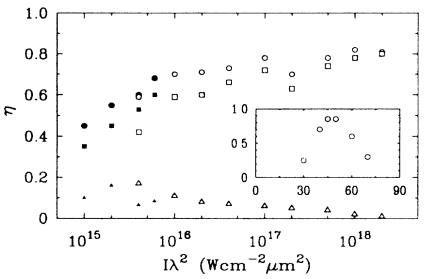

FIG. 4. Final absorption rates vs laser irradiance: total (○), fast electron component (squares), and fast ions (△). The filled symbols indicate simulations with $n_e/n_c = 5$; the open symbols $n_e/n_c = 10$. Inset: final absorption vs angle of incidence at 10^{18} W cm^{-2} μm^2.

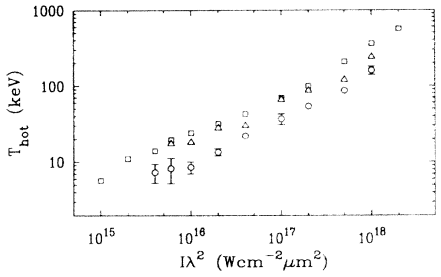

FIG. 5. Temperature of absorbed fast electrons (□), bulk plasma electrons (○), and ions (△).

simulations with $I\lambda^2 \geq 10^{17}$, though the coefficient (at 45°) is about twice that in the above expression. It is instructive to compare this expression with the time scale for "hole punching" due to a finite spot size [11], which is roughly $t_\perp \sim 140\sqrt{A/Z}(v_{\rm osc}/c)^{-1}[r_0/(1\ \mu{\rm m})]$ fs. Thus, for spot sizes $r_0 > 6$ μm, this effect will not be too significant for sub-ps pulses over the intensity range considered here.

The asymptotic steady-state absorption rates are plotted in Fig. 4. Note that the relative ion fraction increases towards lower intensity, making up 15%–20% of the total laser energy for $I\lambda^2 < 10^{16}$. This additional fast ion component and the dips in the solid curve in Fig. 3 suggest that the resonant plasma wave is unstable, exhibiting periodic Langmuir collapse [17], and thus bursts of ion heating. The growth rate for this instability is $\gamma_{\rm max} \simeq \omega_p\sqrt{m_e W/3m_i}$ [17,18], where $W = v_p^2/(n_e/n_c v_{te}^2)$ and v_p is the electron quiver velocity in the plasma wave. For the simulation with $I\lambda^2 = 4\times10^{15}$, we find $v_p \simeq 0.1 \simeq 2v_{\rm osc}$, which at $n_e = n_c$ gives $W = 2$, and thus $\omega_0\gamma_{\rm max}^{-1} \simeq 50$, which is consistent with the typical "collapse" period $\omega_0\tau_c \sim 70$ seen in Fig. 3.

At the high-intensity end, the final absorption rate is over 80%, despite the sharp gradient $L/\lambda \lesssim 0.05$ maintained by the ponderomotive force, and the low shelf density $n_s \lesssim n_c/4$. We find no evidence for surface-wave heating—which would require a shelf of $n_s \sim n_c$ extended over a region $\gtrsim \lambda/2$ [19], or of heating by parametric instabilities (e.g., Raman scattering), in the underdense region [18]. It should be noted that side- and backscattered modes are excluded by the 1D boost technique, but these are unlikely to contribute much owing to the low density and short length [(1–2)λ] of the shelf. The particle orbits are characteristic of vacuum heating, and a dramatic increase in (p_x, x) phase-space density in the vacuum-shelf region is observed between the initial step-profile configuration of Fig. 1, and later times $t \geq t_s$.

Making use of the scaling law of Eq. (1) for the (approximately linear) buildup time, and the fact that the asymptotic absorption rate η_0 in Fig. 4 is more or less intensity independent, we obtain a handy formula for the average absorption of a (square) pulse of finite duration τ_p in the high-irradiance limit ($I\lambda^2 > 10^{17}$):

$$\overline{\eta}(\tau_p) = \begin{cases} \eta_0\tau_p/2t_s, & \tau_p \leq t_s, \\ \eta_0(1 - \frac{t_s}{2\tau_p}), & \tau_p > t_s, \end{cases} \qquad (2)$$

where $t_s(45°) = 130(A/Z)^{\frac{1}{2}}(\lambda_\mu)$ fs and $\eta_0(45°) = 80\%$; A is the atomic mass number of the target. The angular dependence is somewhat complicated because both the buildup time and the final absorption vary with θ. Further simulations give absorption coefficients $\eta_0(30°) = 25\%$ and $\eta_0(60°) = 60\%$, with corresponding buildup times of 270 fs and 70 fs for $A = Z = \lambda_\mu = 1$. For $I\lambda^2 < 10^{17}$ and pulse lengths $\tau_p < t_s$, the average absorption may well be higher than that given by Eq. (2) because the buildup time for resonance absorption (estimated earlier) is less than the value from Eq. (1).

The energies associated with the various plasma electron and ion populations are given in Fig. 5. The suprathermal plasma electron temperatures are generally higher than those obtained for fixed profiles with similar scale lengths [8], presumably due to the presence of the underdense shelf. This implies that the ion mobility parameter $(Z/A)^{1/2}$, or equivalently the ratio τ_p/t_s, also affects the temperature of the suprathermals, as well as their number. For intensities below 10^{17}, these temperatures are also consistent with those obtained in earlier

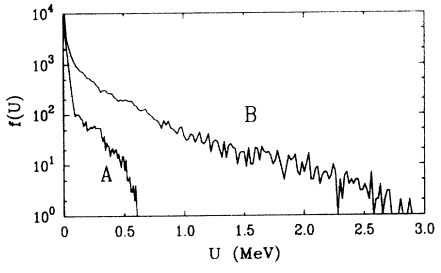

FIG. 6. Time-integrated hot electron spectra for $I\lambda^2 = 10^{18}$ after $t = 2t_s$: fixed ions, curve A; mobile ions with $m_i/Zm_e = 1836$, curve B.

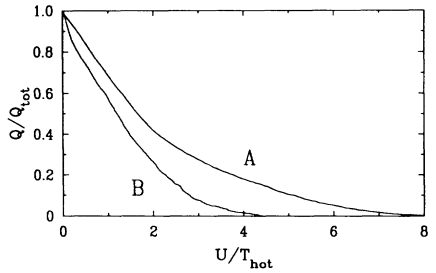

FIG. 7. Self-similar cumulative heat flow for $I\lambda^2 = 10^{18}$ (curve A) and $I\lambda^2 = 4 \times 10^{15}$ (curve B). The quantities Q, $Q_{\rm tot}$, and U are defined in the text.

2D simulations starting from a step profile [16].

The distribution of the *absorbed* fast electrons also gets hotter as the shelf forms, undergoing a transition from a monoenergetic beamlike population ($t \ll t_s$) to a bi-Maxwellian ($t \gtrsim t_s$) similar to that observed in long-scale-length simulations. This effect is illustrated in Fig. 6, which compares the mobile-ion result with the same run for fixed ions at $I\lambda^2 = 10^{18}$. The "temperatures" of these spectra are 250 keV (curve A) and 360 keV (curve B), respectively; the absorption for the fixed-ion run was 10%, as in Ref. [8].

For times $t > t_s$, the cumulative heat flow, defined as $Q(U) = \int_0^U q(U')dU' = m_e c^3 \int_0^U U' f(U')dU'$, where $U = (1 + p_x^2 + p_y^2)^{\frac{1}{2}} - 1$, assumes a self-similar form when normalized to the total energy absorbed $Q_{\rm tot} = \int_0^\infty q(U')dU'$, and plotted against $U/T_{\rm hot}$. This is shown in Fig. 7 for the two simulations considered earlier [$I\lambda^2 = 10^{18}$ (curve A) and $I\lambda^2 = 4 \times 10^{15}$ (curve B)], after a run time $t \simeq 2t_s$. Though these curves are prone to some uncertainty in defining $T_{\rm hot}$ (typically 5%–10% for the data in Fig. 5), there appears to be a clear qualitative difference between the low- and high-intensity cases: The other curves for $I\lambda^2 \geq 10^{17}$ lie more or less on top of curve A; below this there is a smooth transition to curve B. Thus, in the high-intensity limit, over 25% of the absorbed laser energy is carried by electrons with energies $U \geq 3T_{\rm hot}$; for $I\lambda^2 \lesssim 10^{16}$ this fraction is only 10%.

In summary, a comprehensive model of fast electron generation applicable to femtosecond laser-solid interactions has been presented, in which the ion motion and oblique-incidence effects—resonance absorption and vacuum heating—have been taken into account explicitly. For irradiances above $I\lambda^2 \geq 10^{17}$, the absorption rate reaches an optimum final value $\gtrsim 80\%$ for $\theta = 45°$–$50°$, after a buildup phase $t_s = 130(A/Z)^{1/2}\lambda_\mu$ fs associated with the formation of an underdense ion shelf. The overall absorption for a given pulse length thus depends on the laser wavelength and the ionization state Z, which may also vary during the interaction [20]. Most of the energy is carried into the solid by fast electrons, though for $I\lambda^2 \leq 10^{16}$ a significant proportion (10%–20%) goes into shelf ions accelerated away from the target. For Gaussian pulses and higher densities (e.g., $n_e/n_c \sim 100$) the absorption scaling should still hold qualitatively, but may differ numerically because $P_{\rm osc}/P_e$ will be time dependent, resulting in a transition between absorption regimes during the interaction.

The author acknowledges valuable discussions with A.R. Bell, R.P.J. Town, J. Delettrez, and R. Sauerbrey. This work was supported the CEC Human Capital and Mobility Programme.

[1] J. D. Kmetec *et al.*, Phys. Rev. Lett. **68**, 1527 (1992); P. Audebert *et al.*, Europhys. Lett. **19**, 189 (1992); U. Teubner *et al.*, Phys. Rev. Lett. **70**, 794 (1993); H. Chen *et al.*, Phys. Rev. Lett. **70**, 3431 (1993); D. D. Meyerhofer *et al.*, Phys. Fluids B **5**, 2584 (1993); R. Sauerbrey *et al.*, in *Short Wavelengths V* (AIP, San Diego, 1993), Vol. 17, pp. 177–181.
[2] R. L. Carman, D. W. Forslund, and J. M. Kindel, Phys. Rev. Lett. **46**, 29 (1981); S. C. Wilks, W. L. Kruer, and W. B. Mori, IEEE Trans. Plasma Sci. **21**, 120 (1993).
[3] M. M. Murnane, H. C. Kapteyn, M. D. Rosen, and R. W. Falcone, Science **251**, 531 (1991).
[4] M. Tabak *et al.*, Phys. Plasmas **1**, 1626 (1994).
[5] H. M. Milchberg, R. R. Freeman, S. C. Davey, and R. M. More, Phys. Rev. Lett. **61**, 2364 (1988); J. C. Kieffer *et al.*, Phys. Rev. Lett. **62**, 760 (1989); R. Fedosejevs *et al.*, Phys. Rev. Lett. **64**, 1250 (1990).
[6] D. W. Forslund *et al.*, Phys. Rev. A **11**, 679 (1975).
[7] F. Brunel, Phys. Rev. Lett. **59**, 52 (1987); Phys. Fluids **31**, 2714 (1988).
[8] P. Gibbon and A. R. Bell, Phys. Rev. Lett. **68**, 1535 (1992).
[9] J. Delettrez *et al.*, Bull. Am. Phys. Soc. **10**, 1987 (1993).
[10] A. A. Andreev *et al.*, Sov. Phys. JETP **74**, 963 (1992).
[11] S. C. Wilks, W. L. Kruer, M. Tabak, and A. B. Langdon, Phys. Rev. Lett. **69**, 1383 (1992).
[12] J. Denavit, Phys. Rev. Lett. **69**, 3052 (1992).
[13] B. N. Chichkov, Y. Kato, and M. Murakami, Phys. Rev. A **46**, 4512 (1992).
[14] X. Liu and D. Umstadter, Phys. Rev. Lett. **69**, 1935 (1992).
[15] K. G. Estabrook, E. J. Valeo, and W. L. Kruer, Phys. Fluids **18**, 1151 (1975).
[16] K. G. Estabrook and W. L. Kruer, Phys. Rev. Lett. **40**, 42 (1978).
[17] V. E. Zakharov, Sov. Phys. JETP **35**, 908 (1972).
[18] J. C. Adam and A. Héron, Phys. Fluids **31**, 2602 (1988).
[19] J. M. Kindel, K. Lee, and E. L. Lindman, Phys. Rev. Lett. **34**, 134 (1975).
[20] R. Town, A. Bell, and S. Rose, Phys. Rev. E (to be published).